

Structure, Kinematics, and Chemical Enrichment Patterns after Major Gas-Rich Disc-Disc Mergers

Simon Richard,^{1,2,3} Chris B. Brook,⁴ Hugo Martel,^{1,3} Daisuke Kawata,⁵
 Brad K. Gibson,⁴ and Patricia Sanchez-Blazquez^{4,6,7}

¹*Département de physique, de génie physique et d'optique, Université Laval, Québec, QC, G1K 7P4, Canada*

²*Hubert Reeves Fellow*

³*Centre de Recherche en Astrophysique du Québec*

⁴*Jeremiah Horrocks Institute for Astrophysics & Supercomputing, University of Central Lancashire, Preston, PR1 2HE, UK*

⁵*Mullard Space Science Laboratory, University College London, Holmbury St. Mary, RH5 6NT, UK*

⁶*Instituto de Astrofísica de Canarias, E-38200 La Laguna, Tenerife, Spain*

⁷*Departamento de Astrofísica, Universidad de La Laguna, E-38205 La Laguna, Tenerife, Spain*

ABSTRACT

We used an N-body smoothed particle hydrodynamics algorithm, with a detailed treatment of star formation, supernovae feedback, and chemical enrichment, to perform eight simulations of mergers between gas-rich disc galaxies. We vary the mass ratio of the progenitors, their rotation axes, and their orbital parameters and analyze the kinematic, structural, and chemical properties of the remnants. Six of these simulations result in the formation of a merger remnant with a disc morphology as a result of the large gas-fraction of the remnants. We show that stars formed during the merger (a sudden starburst occur in our simulation and last for 0.2 – 0.3 Gyr) and those formed after the merger have different kinematical and chemical properties. The first ones are located in thick disc or the halo. They are partially supported by velocity dispersion and have high $[\alpha/\text{Fe}]$ ratios even at metallicities as high as $[\text{Fe}/\text{H}] = -0.5$. The former ones – the young component – are located in a thin disc rotationally supported and have lower $[\alpha/\text{Fe}]$ ratios. The difference in the rotational support of both components results in the rotation of the thick disc lagging that of the thin disc by as much as a factor of two, as recently observed. We find that, while the kinematic and structural properties of the merger remnant depends strongly upon the orbital parameters of the mergers, there is a remarkable uniformity in the chemical properties of the mergers. This suggests that general conclusions about the chemical signature of gas-rich mergers can be drawn.

Key words: galaxies: formation — galaxies: evolution — galaxies: interactions — galaxies: structure

1 INTRODUCTION

1.1 Disc-Disc Mergers

In a Λ Cold Dark Matter Universe (Λ CDM), the formation of structures generally involves the merging of smaller structures. Mass is built up predominantly by the merger of objects of masses between 3 – 30% of the galaxy’s total mass at redshift $z = 0$ (Stewart et al. 2008). Since $z = 2$, approximately 60% of galaxies have experienced a major merger, which we will take in this paper as those involving a ratio of masses 3:1 or higher. Also, an important fraction of the baryonic mass (30 - 50%) of $z = 0$ galaxies is provided by major mergers (Stewart et al. 2009). Recent observations show that nearly 20% of the massive disc galaxies have un-

dergone a major merger since $z \sim 1.5$ (López-Sanjuan et al. 2009) This process is virtually scale-free, meaning that low-mass dark matter halos, in which disc galaxies presumably reside, have undergone similar merging histories to high-mass dark matter halos in which, predominantly, ellipticals reside. This at first is puzzling, as mergers have long been associated with forming spheroidal structures, i.e. early-type galaxies (Toomre 1977). Following this line of reasoning, every galaxy in the nearby universe should be an elliptical or an irregular, which is clearly not the case. Furthermore, observed elliptical galaxies can be described by simple relations relating colors, luminosities, masses, etc. These simple relations are difficult to reproduce with a scenario involving collisions (Bekki & Shioya 1998, 1999).

The resolution of this, of course, lies with the baryonic

physics. Studies using two stable discs as initial conditions (Springel & Hernquist 2005; Robertson et al. 2006; Brook et al. 2007, hereafter B07; Robertson & Bullock 2008) as well as fully cosmological simulations (Governato et al. 2008) have shown that binary gas-rich mergers can result in disc morphologies. Hence, major mergers between gas-rich disc galaxies can possibly play an important role in the formation of a large number of the spiral galaxies we observe today. These facts bring an addition to the original scenario for the formation of disc galaxies, which involved the assembly of a halo of dark matter and ionized gas by hierarchical clustering and mergers of sub-halos, followed by the collapse and virialization of the dark matter halo, and finally the dissipative collapse of the baryonic component, resulting in a rotationally-supported disc, that will later fragment to form stars (White & Rees 1978; Fall & Efstathiou 1980; Blumenthal et al. 1984).

One must also consider a formation scenario involving major collisions between spiral galaxies. The first numerical simulations of major collisions between disc galaxies were performed under the assumption that dissipation by gasdynamical effects was negligible. The results showed that the remaining galaxy had several properties attributed to elliptical galaxies, including luminosity profiles (Naab & Burkert 2003; Barnes 2002; Barnes & Hernquist 1992; Hernquist 1992, 1993; Bekki & Shioya 1998, 1999; Naab, Burkert, & Hernquist 1999). Even with the quite recent inclusion of feedback processes, the results remained mostly unchanged (Barnes & Hernquist 1996; Mihos & Hernquist 1996; Springel 2000; Naab et al. 2006). Minor collisions have also been studied in the past and results showed that this kind of collision tends to form galaxies whose disc is destroyed or very perturbed (Hernquist & Mihos 1995; Bekki 1998). All the aforementioned studies assumed a ratio gas/stars more representative of present low redshift mergers. Of course, stars have not always been present inside galaxies. Going back in time, we can expect to find fewer and fewer stars, and therefore a more important gaseous component (Stewart et al. 2009).

1.2 Thick Discs

The Milky Way’s thick disc is made predominantly of old stars, with ages in the range of 8 – 12 Gyr, significantly older than the typical star found in the thin disc (Gilmore, Wyse, & Jones 1995). The thick and thin disc differ in their structural, chemical, and kinematical properties: (1) The thick disc has a scale height of about 900 pc, compared to 300 pc for the thin disc (Jurić et al. 2008). (2) The stars in the thick disc have a low metallicity, $[\text{Fe}/\text{H}] \sim -0.6$ on average, and a ratio $[\alpha/\text{Fe}]$ larger than the stars in the thin disc. (3) Stars in the thick disc tend to rotate slower than stars in the thin disc, by about 40 km s^{-1} (Gilmore, Wyse, & Kuijken 1989) and have an average vertical velocity dispersion of 45 km s^{-1} compared to $\sim 10\text{--}20 \text{ km s}^{-1}$ for the stars in the thin disc (Delhaye 1965; Chiba & Beers 2000).

The formation of the Milky Way’s thick disc remains an open question, with popular theories including the heating of a thin disc by minor mergers (Quinn, Hernquist, & Fullagar 1993; Kazantzidis et al. 2008; Kazantzidis, Zentner, & Bullock 2008), or the direct

accretion of stars, which are tidally torqued into the plane of the existing thin disc (Abadi et al. 2003), or dynamical heating by destruction of very massive star clusters (Kroupa 2002; Elmegreen & Elmegreen 2006). We favor a scenario in which the Milky Way’s thick disc is formed during the high-redshift epoch in which mergers are most common in ΛCDM , and accretion rates are high, with the disc which formed during this turbulent period being born thick; the thin disc subsequently grows during the relatively quiescent period which follows, which in the case of the Milky Way is approximately the last 10 Gyrs (Brook et al. 2004b, 2005, 2006).

Recent observations suggest that all spiral galaxies are surrounded by a red, flattened envelope of stars, and these structures have been interpreted as showing that thick discs are ubiquitous in spiral galaxies (Dalcanton & Bernstein 2002). Hence, understanding the formation of the thick disc will provide major insights into the formation processes of spiral galaxies. If we make the hypothesis that thick disc are formed during gas-rich major mergers, it would mean that a significant number of spiral galaxies have experienced major mergers. Indeed, simulations have shown that gas-rich mergers tend to form two disc components (Robertson et al. 2006; B07). These simulations included the effect of star formation and supernovae feedback, which allowed to study the kinematical and structural properties of galaxy merger remnants in detail. However, they did not include a detailed treatment of chemical enrichment and, therefore, could not predict the abundances of metals in stars and the interstellar medium (but see also Bekki & Shioya 1998, 1999, who studied the formation of elliptical galaxies due to a more violent major merger). It is well-established that the thick disc of the Milky Way possesses a unique chemical signature, which is believed to be directly related to the formation process and it is important to analyze if the merger scenario for the formation of the thick disc component is compatible with these chemical signatures. This is the basis of our study here: we believe that the remnants of major mergers may be associated with a significant fraction of the “red envelopes” observed in Dalcanton & Bernstein (2002), i.e. with extragalactic thick discs. Since we expect the conditions for merging galaxies during hierarchical clustering at a high redshift to vary, we need to consider a wide range of parameters, such as mass ratio, orbit, and gas fraction of the merger progenitors. In this paper, we present a series of 8 simulations of mergers of gas-rich disc galaxies, with different mass ratios and orbital parameters. We analyze the kinematic and structural properties of the merger remnants. The results for one of the simulations have already been presented in a previous paper (B07). We now complete this work by presenting the entire suite of simulations.

For kinematic properties, we determine the relative importance of rotation and velocity dispersion in providing support. We also investigate if a counter-rotating component arises naturally in a gas-rich merger, as such components are observed in nature (Yoachim & Dalcanton 2006). For structural properties, we determine if the luminosity profiles of these thick discs formed in major mergers follow an exponential law, and if so, what their respective scale lengths are. We determine if the thick and thin discs in merger remnants are coplanar, or if there is a significant angle between them, something that was not included in our previous work.

However, the main goal of the present paper is to study the viability of the merger mechanism for the formation of the thick disc from the chemical evolution's point of view, but without neglecting the kinematical and dynamical properties. With this in mind, we choose initial conditions likely to produce a discy remnant.

In this paper, we use the numerical algorithm GCD+, which includes a detailed treatment of chemical enrichment, to investigate whether key abundance ratios such as $[\alpha/\text{Fe}]$ and $[\text{Fe}/\text{H}]$ in simulated remnants of gas-rich disc galaxy mergers have values and distributions similar to the ones found in the observed disc galaxies, including the Milky Way.

The remainder of this paper is organized as follows: in §2, we briefly describe the numerical simulations employed, including the N-body/SPH code adopted (GCD+), the initial conditions software (GalactICS), and the basic parameters of our 8 realizations. The kinematical and structural properties of the merger remnants are presented in §3 and discussed in §4. Conclusions are presented in §5.

2 THE NUMERICAL SIMULATIONS

2.1 The Algorithm

All simulations were performed using GCD+ (Kawata & Gibson 2003a,b), self-consistently modeling the effects of gravity, gas dynamics, radiative cooling, and star formation. GCD+ is a Tree/SPH algorithm that includes Type Ia and Type II SNe feedback, and traces the lifetimes of individual stars, enabling us to monitor the chemical enrichment history of our simulated galaxies. Star formation occurs in a convergent gas velocity field where gas density is greater than a critical density, $\rho_{\text{crit}} = 2 \times 10^{-25} \text{ g cm}^{-3}$. The star formation rate (SFR) of eligible gas particles is then $d\rho_*/dt = d\rho_g/dt = c_*\rho_g/t_g$ where $c_* = 0.05$ is a dimensionless star formation efficiency, and t_g is the dynamical time. This formula corresponds to a Schmidt law: $\text{SFR} \propto \rho^{1.5}$. The mass, energy, and heavy elements are smoothed over the neighboring gas particles using the SPH smoothing kernel. The code separately tracks the abundances of 9 elements: H, He, C, N, O, Ne, Mg, Si, and Fe. Gas within the SPH smoothing kernel of Type II SNe explosions is prevented from cooling, creating an adiabatic phase for gas heated by such SNe. This adiabatic phase is assumed to last for the lifetime of the lowest mass star that ends as a Type II SNe, i.e., the lifetime of an $8M_\odot$ star (100 Myr). This is similar to a model presented in Thacker & Couchman (2000). Stellar yields are dependent of the progenitor mass and metallicity. For Type II SNe, we use the metallicity-dependent stellar yields of Woosley & Weaver (1995) for stars with mass over $11M_\odot$, while for low- and intermediate-mass stars, we use the stellar yields of van den Hoek & Groenewegen (1997). For Type Ia SNe, we adopt the model of Kobayashi, Tsujimoto, & Nomoto (2000) in which Type Ia SNe occur in binary systems with a primary star and a companion of a definite mass and metallicity range. The yields are from Iwamoto et al. (1999). Note that GCD+ relaxes the instantaneous recycling approximation and takes into account the lifetime of progenitor stars, and chemical enrichment from intermediate mass stars. The

code calculates, within each timestep, the amount of energy and heavy element released by every star particle and distributes them over the neighbours using the SPH kernel for both Type II and Ia SNe. We did not include in the present paper any black hole feedback. Several studies have demonstrated that this can be very important for the final morphology and the termination of the star formation in the merger remnant (Springel, Di Matteo & Hernquist 2005; Okamoto et al. 2005; Johansson et al. 2009). However, the implementation of the blackhole feedback in numerical simulations is still highly ambiguous and we prefer here, for simplicity, to include only SN feedback. For more details about GCD+, we refer the reader to Kawata & Gibson (2003a,b); Brook et al. (2004a).

2.2 Setting Up Initial Conditions

In each simulation, the initial conditions consist of two galaxies with exponential gas discs embedded in dark matter halos. These galaxies are generated using the GalactICS package (Kuijken & Dubinski 1995), producing stable discs for a large number of galactic rotations. For the dark matter halos, GalactICS use the lowered Evans model (Evans 1993), which leads to a constant-density core. This model differs from models which have a steeper central density profile suggested by ΛCDM cosmological simulations (Navarro, Frenk, & White 1996, 1997; Moore et al. 1999; Ghigna et al. 2000; Jing & Suto 2000; Klypin et al. 2001). For our purpose this difference is not critical, as the central regions contain only a small fraction of the total mass. The star formation mechanism is shut down for the first $\sim 180\text{Myr}$ enabling very gas-rich mergers. In our simulations, the gas ratio immediately before merger is more relevant than the initial value. Pure gas disc will induce an unrealistic starburst initially. However, by turning off star formation initially, we can control the gas fraction at the merger epoch. For each simulation, the most massive galaxy (Gal1) has total mass of $5 \times 10^{11}M_\odot$ (except for simulation M11) and a scale length of 4.5 kpc. The mass and scale length of the second galaxy (Gal2) depends on the specific mass ratio chosen for the simulation. Using the observed gas fraction of galaxies at high (Erb et al. 2006) and low (McGaugh 2005) redshift, Stewart et al. (2009) provide a relation between gas fraction and redshift for galaxies of various masses. Using this relation (their equation [1]) allows us to estimate that the mergers in the epoch between $z = 2.37 - 3.7$ would be between galaxies which have gas fractions as high as the ones used in our study. Note that this is an upper bound of such epoch due to the fact that the high redshift observations of Erb et al. (2006) are considered lower bounds of the gas content. Also, these redshifts coincide with the epoch of formation of the stars in the Milky Way thick disc.

The initial configuration of the system is illustrated in Fig. 1. Gal1 is initially located at $\mathbf{R}_1 = (50, 0, 0)\text{kpc}$, with no initial velocity, and its rotation axis pointing in the Z direction. Gal2 is located at $\mathbf{R}_2 = (0, 0, 15)\text{kpc}$ (except for simulations M12C and M12orb), with initial velocity $\mathbf{V}_2 = (0, 100, 0)\text{km s}^{-1}$ (except for simulation M12z), and its rotation axis in the $X - Z$ plane at an angle θ relative to the Z -axis. We shall refer to this angle as the *interaction angle*.

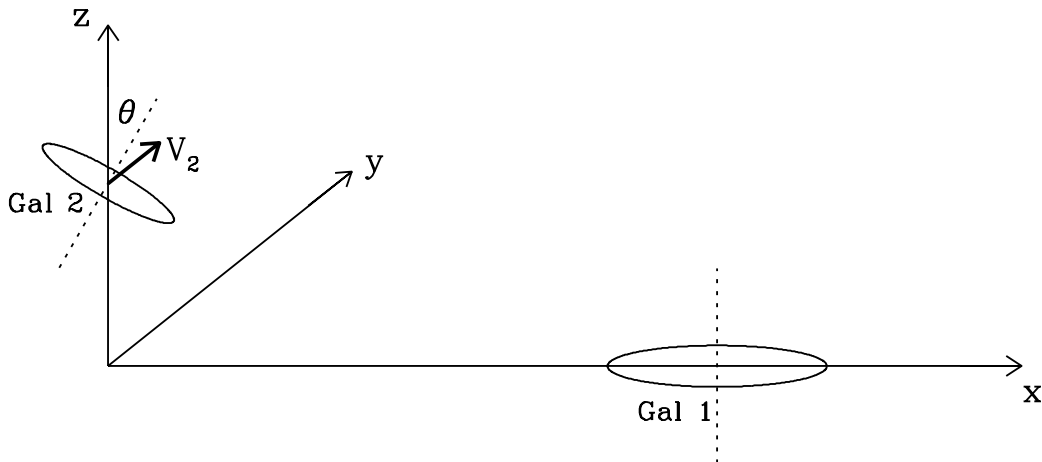


Figure 1. Geometry of the initial conditions. The Y-axis is pointing away from the viewer. Gal1 is initially at rest, while Gal2 is initially moving away from the viewer, in the +Y direction, as the thick arrow shows. The dotted lines indicate the rotation axes of the galaxies. Gal1 is in the X – Y plane, with the rotation axis in the Z-direction. The rotation axis of Gal2 is in the X – Z plane, at an angle θ relative to the Z-axis. Both galaxies are rotating clockwise when seen from above, hence the left edges are moving away from the viewer, and the right edges are moving toward the viewer. The particular case shown on this figure corresponds to simulation M12, with the edges of the discs located at two scale-lengths.

All encounters are prograde-prograde, except for simulation rM12, for which the rotation of Gal2 is retrograde.

2.3 A Series of 8 Gas-Rich Mergers

We have performed a total of 8 simulations with different initial conditions, in which each galaxy is modeled using 100,000 dark matter halo particles and 40,000 gas particles, for a total of 280,000 particles. This resolution is lower by a factor 2 than the one used in Robertson et al. (2006). Since the primary goal of this work is to experiment on chemical enrichment following a major merger, we had to make some choices relative to the numerical resolution we had to use. The primary concern being the relatively high computation time needed to distribute enrich gas to the particles in the neighborhood. The baryon/DM mass fraction is 17%, which is equal to the universal ratio Ω_b/Ω_0 according to recent estimates (Spergel et al. 2007; Komatsu et al. 2009). Every simulation starts with an initial metallicity $\log(Z/Z_\odot) = -4$ and α -element abundance $[\alpha/\text{Fe}] = 0.30$.

Table 1 lists the parameters used for generating the initial conditions for each simulation. The five simulations within the M12 “family” involve a major merger of two galaxies with a mass ratio of 2:1. We start with M12, which has already been discussed in detail in B07. The galaxies collide after 320 Myr, and by that time 6% of the gas has already been converted to stars, leaving a gas fraction $f_{\text{gas}} = 0.94$. The next 4 simulations within that family are variations of the “parent” simulation M12. In simulation M12orb, we increase the initial separation between the galaxies, and in simulation M12z, we add an additional velocity component in the z-direction. In both cases, the merger is delayed, and this results in lower gas fractions at the time of the merger. In simulation M1290 we changed the interaction angle to 90 degrees. Simulation rM12 is similar

to simulation M12, except that the direction of rotation of Gal2 is reversed, making it retrograde relative to the orbit.

With the last 3 simulations, we consider different mass ratios. In simulation M11, we used equal-mass galaxies. Also, this simulation is the only one for which we use a smaller mass for Gal1: $2.5 \times 10^{11} M_\odot$ instead of $5 \times 10^{11} M_\odot$. In simulation M13, we use a mass ratio of 3:1. This is still considered to be a major merger. In the simulation M110, we use a mass ratio of 10:1, which corresponds to a minor merger.

Column 8 of Table 1 gives the initial eccentricities of the orbits. Except for simulation M110 (the minor merger), the eccentricities are quite high, corresponding to elongated elliptical orbits. As a result, the pericenters are smaller than the actual size of the galaxies, and the collision takes place before a full orbit is completed. Column 9 gives the angle between the position of the pericenter and the line of nodes (intersection between the orbital plane and the plane of Gal1; see p. 632 of Toomre & Toomre 1972). Column 10 gives the inclination ι of Gal2 relative to the plane of the orbit.

For the simulation M11, the softening length of the algorithm is 0.65 kpc for the dark matter and 0.48 kpc for the baryons. For the other simulations, the softening length is 0.82 kpc for the dark matter and 0.61 kpc for the baryons.

Table 2 lists the time t_f elapsed between the beginning and the end of the simulation, the time t_{coll} elapsed between the beginning of the simulation and the collision, and the final gas fraction $f_{\text{gas}}^{\text{final}}$. In each simulation, the collision leaves a very complex and chaotic system, which then relaxes to a “quiescent state” where the final structure and kinematics are well-established, and the star formation rate has dropped significantly. We stopped the simulations after 2.5 Gyrs, when the quiescent state had been reached. One simulation (M12orb) was extended to $t_f = 3.40$ Gyrs, which enabled us to check that the final state was indeed quiescent. Comparing the values of $f_{\text{gas}}^{\text{final}}$ with the values of f_{gas}

Table 1. Initials Conditions for All Simulations

Run	$M_{\text{Gal}}(M_{\odot})$	mass ratio	f_{gas}	θ	V_{2z} (km s $^{-1}$)	R_2 (kpc)	e	ω [degree]	i [degree]
M12	5.0×10^{11}	2:1	0.94	30.0	0	0, 0, 15	0.79	90	-13
M12orb	5.0×10^{11}	2:1	0.67	30.0	0	0, 50, 15	0.86	51	-13
M12z	5.0×10^{11}	2:1	0.83	30.0	100	0, 0, 15	0.66	29	-20
M1290	5.0×10^{11}	2:1	0.96	90.0	0	0, 0, 15	0.91	90	73
rM12	5.0×10^{11}	2:1	0.91	210.0	0	0, 0, 15	0.79	90	167
M11	2.5×10^{11}	1:1	0.88	30.0	0	0, 0, 15	0.89	90	-13
M13	5.0×10^{11}	3:1	0.92	30.0	0	0, 0, 15	0.70	90	-13
M110	5.0×10^{11}	10:1	0.85	30.0	0	0, 0, 15	0.37	90	-14

Table 2. Lookback Times and Final Gas Fraction

Run	t_f [Gyrs]	t_{coll} [Gyrs]	$f_{\text{gas}}^{\text{final}}$
M12	2.50	0.27	0.14
M12orb	3.40	0.83	0.18
M12z	2.50	0.50	0.20
M1290	2.50	0.25	0.10
rM12	2.47	0.32	0.18
M11	2.50	0.40	0.06
M13	2.50	0.32	0.18
M110	2.50	0.42	0.30

listed in Table 1 reveals the efficiency of the starburst in converting gas to stars. The gas fraction typically dropped from $\sim 90\%$ to $\sim 15\%$. It is interesting to note that simulation M110, the only case of a minor merger, was less efficient in converting gas to stars than the other simulations, with $f_{\text{gas}}^{\text{final}} = 0.297$.

3 RESULTS

Following the approach of Robertson et al. (2006), we have computed the SFR for all the simulations, and used these results to identify stellar populations. Some examples of them are shown in the top left panels of Figs. 6–9. Notice that the simulations start at $t = 0$. The results are quite similar for all simulations. A major starburst invariably occurs during the merger. This starburst peaks between $\sim 60M_{\odot} \text{ yr}^{-1}$ and $500M_{\odot} \text{ yr}^{-1}$, comparable to that seen in high-redshift Lyman-break galaxies (Erb et al. 2006). The results are qualitatively similar to recent work involving similar gas ratio but different feedback assumptions (Johansson et al. 2009) or different gas ratio and different feedback (Cox et al. 2008). The main quantitative difference come from the amount of gas available during the merger. As stated in Johansson et al. (2009, see their Figs. 1 and 3), there is a huge difference in the maximum value of the SFR depending on gas mass fraction. The SFR is also dependent of the numerical methods used for feedback in case of major mergers (Cox et al. 2006). After the starburst, the star formation steadily drops, as the system relaxes and a disc forms. We identify the beginning and the end of the merger with the beginning and the end of the starburst, respectively. We then define two populations of stars: *old stars*, which include stars already present in the galaxies before the merger and stars formed during the merger by the starburst, and *young stars*, which include all stars formed after the merger,

when the starburst is completed. The definitions for young and old stars remain the same throughout the paper. The dashed vertical lines in the top-left panels of Figs. 6–9 indicate the beginning and end of the starburst, identified by eye as the merger boundaries are not crucial for the subsequent analysis. The time when the starburst begins is listed in Table 2. For most simulations, the starburst lasts 0.2–0.3 Gyr. The simulation M12z (Fig. 7) is a notable exception, with a starburst that is weaker and lasts for 0.5 Gyr.

We use the term *remnant* to designate the final state of each simulation. Our simulations are meant to represent the interactions occurring at high redshift, when the gas content is very high. In this sense, the merger remnant represents objects at $z \sim 2-3$ and the galaxies still have time to form more stars until $z = 0$. The subsequent infall of extragalactic gas may also produce more stars at $z = 0$ and help to reform a disc (Brooks et al. 2009).

3.1 Structure and Density Profiles

At the end of each simulation, we calculated the V-band luminosity of the merger remnant, using the stellar synthesis model of Kodama & Arimoto (1997). From this, we produced mock V-band luminosity maps (modulo the lack of dust extinction). Figs. 2–4 show the luminosity maps for 3 remnants. On each figure, the left panels show the stars born after the merger (young stars), the middle panels show the stars born before or during the merger (old stars) and the right panels show all stars.

We immediately see that old and young stars have very different distributions. In simulation M12 (Fig. 2), young and old stars form discs that have comparable radii, but the edge-on views (bottom panels) clearly shows that the young disc is thin, while the old disc is thick. The presence of two distinct discs, a thin one and a thick one, is in remarkable agreement with observations (Yoachim & Dalcanton 2006), and this motivated us to publish the results of that particular simulation in an earlier paper (B07). We found that all the simulations except for simulations M12z and M11 do result in the formation of a thin disc made of young stars, and a thick disc made of old stars that were already present before the merger, or formed during the mergers. These stars end up either in the thick disc or in the halo.

Simulations M12z and M11 show more elliptical like remnants. Simulation M12z (Fig. 3) produced a remnant that has a very complex structure. Even though we find a small disc made of young stars, the overall structure resembles more an elliptical galaxy than a disc galaxy. Simulation M11 also shows a small young disc. Compared with the other

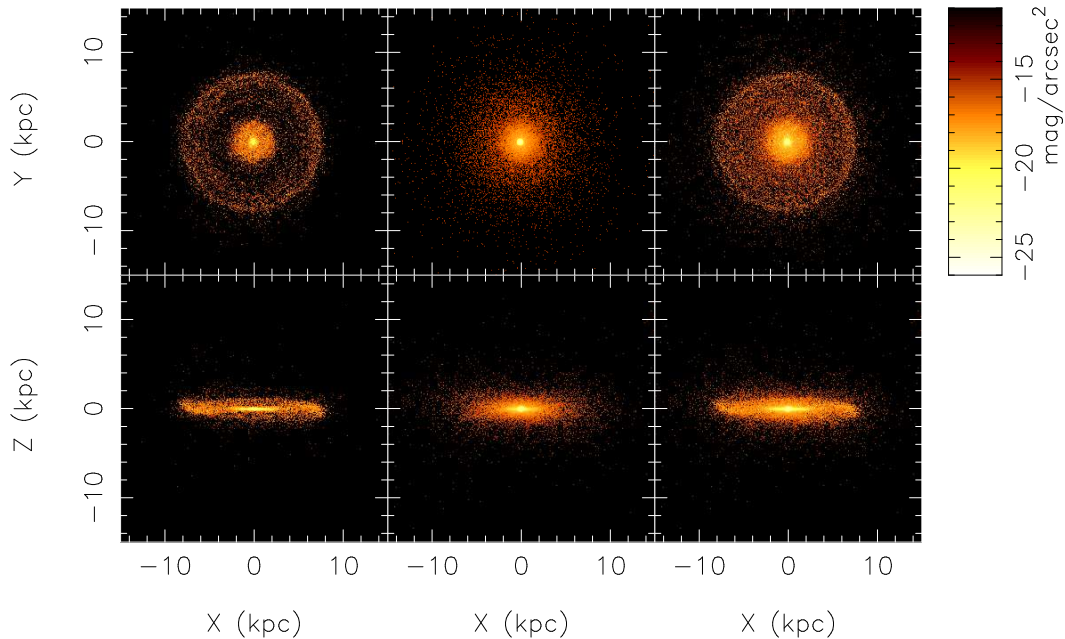


Figure 2. V-band image of M12 seen face-on (top panels) and edge-on (bottom panels), for young stars (left panels), old stars (middle panels), and all stars (right panels). X , Y , Z represent cartesian coordinates, with Z along the axis of rotation.

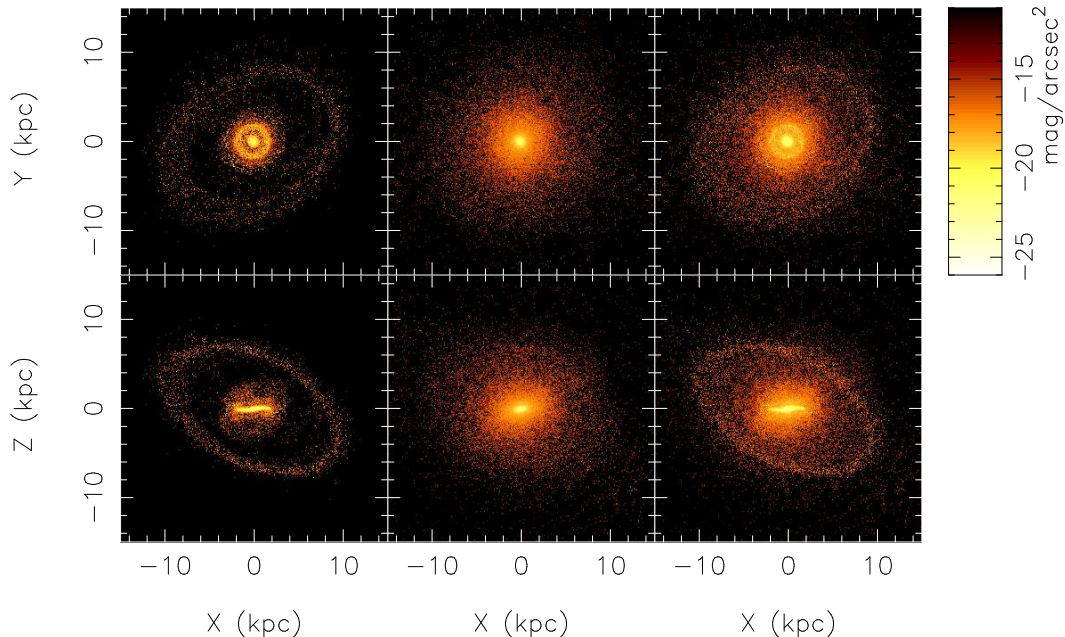


Figure 3. V-band image of M12z seen face-on (top panels) and edge-on (bottom panels), for young stars (left panels), old stars (middle panels), and all stars (right panels). The gas shows a complex structure that lasts for several hundred million years.

simulations, the initial galaxies Gal1 and Gal2 are less massive in simulation M11, but the intensity of the starburst taking place during the merger is comparable. As a result, there is less gas available after the merger to form young stars and build up an extended thin disc.

In most simulations, the merger resulted in the formation of a ring made of young stars. This implies that prograde gas-rich major mergers have a tendency to form rings. These rings seem to be signatures of a gas substructure since

most of the rings are coplanar with the thin disc. The large impact parameter use here is quite contrary to the normal scenarios forming a ring remnant (Hernquist & Weil 1993; Mapelli et al. 2008). That can be a signature of a gas-rich merger, and more work is needed to certify this assertion. The simulation M12z formed a very complex structure, with a non-coplanar ring connected to a very small thin disc by spiral arms, embedded in an ellipsoid distribution of old stars (Fig. 3). Also, the face-on views of the mergers for

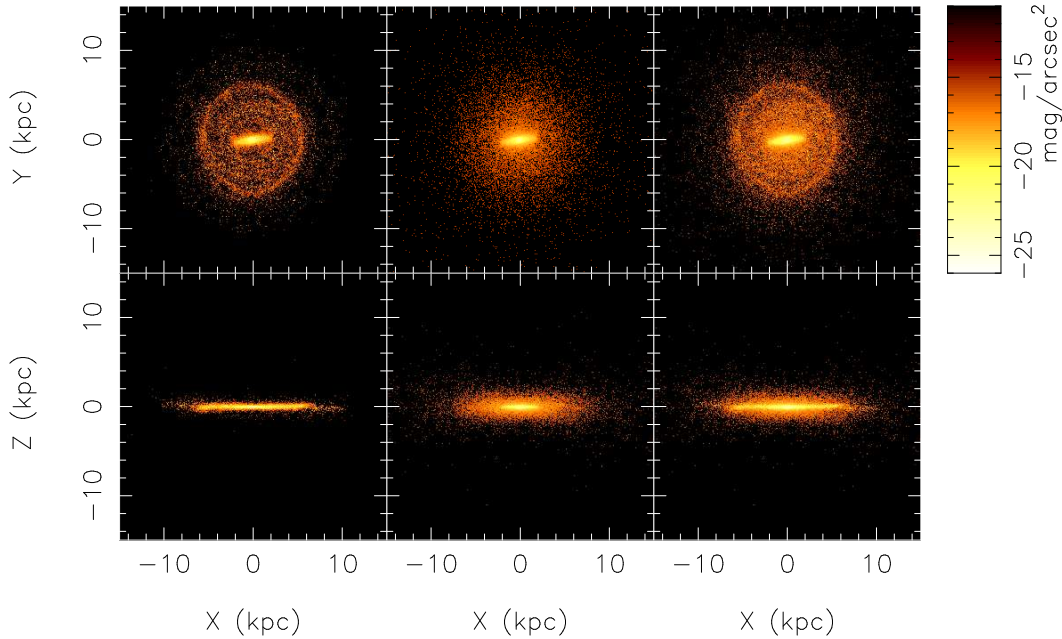


Figure 4. V-band image of M1290 seen face-on (top panels) and edge-on (bottom panels), for young stars (left panels), old stars (middle panels), and all stars (right panels). For this simulation, the stellar ring and the disc are not coplanar.

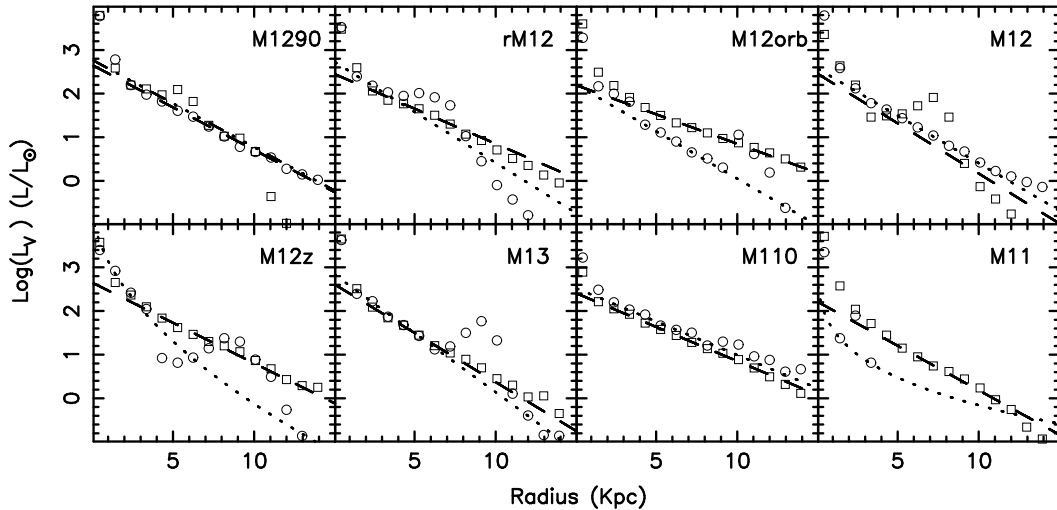


Figure 5. Radial luminosity profile in the V-band, for old stars (squares) and young stars (circles). The straight lines show exponential fits of the old stars (dashed) and young stars (dotted). The dotted curves for simulation M12z and M11 are fits to a de Vaucouleurs profile for the young stars.

simulations M1290 and rM12 (top panels of Figs. 4 for an example) clearly reveal the presence of a central bar made of both old and young stars. No bars are seen in the other simulations.

We can use the surface density brightness to trace the radial luminosity profiles of the discs. The radial luminosity profiles are shown in Fig. 5, for all simulations. We calculated these profiles separately for young stars and old stars. The dotted and dashed lines are fits to the profiles of young and old stars, respectively. In cases where a ring was clearly visible, we excluded it from the fit. All profiles are well-fitted by an exponential profile, except for simulations M12z and

M11, where the young stars are better-fitted by a de Vaucouleurs profile. We can use the exponential profiles to calculate the scale-lengths of the discs. In Table 3, we list the scale-length h_o of the old population, the scale-length h_y of the young population, and their ratio h_o/h_y , except for the simulations M12z and M11, for which an exponential profile does not fit the distribution of young stars. The scale-length is usually larger for the old population than the young one, with ratios varying from 0.98 to 1.60. This is in agreement with the recent observational work to Yoachim & Dalcanton (2006) if we make a direct correspondence between old stars and thick-disc stars.

Table 3. Scale-length ratio for the young and old populations

Run	h_o [kpc]	h_y [kpc]	h_o/h_y
M12	5.56	5.27	1.06
M1290	6.22	6.05	1.03
M12orb	8.97	5.59	1.60
M12z	6.55
rM12	7.54	5.21	1.45
M11	5.94
M13	5.37	4.47	1.20
M110	7.71	7.87	0.98

By definition, by the time the merger is completed, old stars have all formed, while the matter destined to form young stars is still in the form of gas. Hydrodynamical processes, such as oblique shock waves, can potentially exert a torque on the gas, modifying its angular momentum. Such processes would not affect the old population directly, only indirectly through the gravitational interaction between the old stars and the remaining gas. This might result in a misalignment between the young and old discs. To investigate this issue, we performed a least-square fit of a plane to the final distribution of young stars, and to the final distribution of old stars. The second column of Table 4 shows the angle θ_{oy} in degrees between the two planes, that is, the angle between the young and old discs. The angles are 6° or less for all the runs, indicating that the discs tend to be coplanar. To estimate whether these angles are significant, we fitted the distribution of stars in the old disc using an oblate ellipsoid. We then calculated a *relevance angle* θ_o , defined as the arc tangent of the short-to-long axis ratio of the ellipsoid. If we were to fit the old disc inside a flat square box, θ_o would be the angle between the edge and the corner, as seen from the center, so it is a measure of how thick the old disc is. If $\theta_{oy} < \theta_o$, then the young disc is entirely embedded inside the old disc, in spite of the angle between them. But if $\theta_{oy} > \theta_o$, then the young disc “sticks out” of the old disc. The third column of Table 4 shows the relevance angles. Interestingly, the simulation rM12, the only one for which one galaxy is spinning in the retrograde direction, produces an old disc that is actually over an order of magnitude thinner than the ones produced by the other simulations. It is well-known that a retrograde disc will suffer very little tidal disruption prior to merger compared to a prograde disc (Toomre & Toomre 1972). This could explain why the old disc in simulation rM12 ends-up being quite thin, though a more detailed investigation is needed to confirm this hypothesis. The last column of Table 4 shows the ratio θ_{oy}/θ_o . We find that all cases except rM12 have $\theta_{oy}/\theta_o < 1$. Hence, young discs tend to be embedded inside old discs.

3.2 Kinematics

We have analyzed the kinematic properties of all 8 remnants. We computed the rotation curves of the old and young populations, for all the remnants. The top right panels of Figs. 6–9 show some examples of these curves. For simulations M12, M12orb, M1290, rM12, M13, and M110, the old populations have a lower mean rotational velocity than their younger counterparts. The difference is about $200 - 300 \text{ km s}^{-1}$ for

Table 4. Angle between the plane of the disc for by the young and old populations

Run	θ_{oy} [degrees]	θ_o [degree]	θ_{oy}/θ_o
M12	3.28	17.62	0.19
M1290	0.70	11.19	0.06
M12orb	3.26	20.64	0.16
M12z	6.00	41.17	0.78
rM12	2.21	1.27	1.74
M11	2.31	26.68	0.08
M13	5.63	17.82	0.32
M110	0.25	13.80	0.02

M12, M12orb, and M1290 (mass ratio 2:1), 150 km s^{-1} for M13 (mass ratio 3:1) and 50 km s^{-1} for M110 (mass ratio 10:1). Hence, it decreases with increasing mass ratio of the progenitors. Comparing M12 with rM12, we also find that reversing the rotation of Gal2 (so that it is retrograde relative to the orbit of the galaxies) also reduces the differences between the two populations (about 300 km s^{-1} for M12 versus 150 km s^{-1} for rM12). The rotation curve of M12z and M11 are drastically different. The young population of the outer ring is counter-rotating with respect to the young population of the outer disc. We also found some counter-rotating stars in other simulations, but (i) they belong to the old population, and (ii) these stars were in the minority, so the overall rotation curve showed no counter-rotation.

To estimate the relative importance of rotation and velocity dispersion in providing support against gravity, we calculated for each population the average rotational velocity V and its dispersion σ_V in radial bins. The middle left panels of Figs. 6–9 the quantity $\langle (V/\sigma_V)^2 \rangle^{1/2}$ versus radius, for some of the remnants. In all simulations, we find $\langle (V/\sigma_V)^2 \rangle^{1/2} > 1$ for the young population, indicating that this population forms a massive, rotationally supported disc. The only exception is simulation M12z, where $\langle (V/\sigma_V)^2 \rangle^{1/2} < 1$ between radii 3 and 6 kpc. As the top panel of Fig. 7 shows, this region corresponds to the discontinuity between the inner disc and the counter-rotating outer ring. Simulations M12, M12orb, M12z, and M11 all have $\langle (V/\sigma_V)^2 \rangle^{1/2} < 1$, indicating the presence of a “hot disc” supported by internal motions rather than rotation. Simulation M13 has $\langle (V/\sigma_V)^2 \rangle^{1/2} < 1$ at radii $r < 3$ kpc and $\langle (V/\sigma_V)^2 \rangle^{1/2} > 1$ at larger radii. Simulations M1290, rM12, and M110 all have $\langle (V/\sigma_V)^2 \rangle^{1/2} > 1$, indicating that the old population is also rotationally supported, but in all three cases the rotational support is significantly smaller for the old population, typically by a factor of order 5. In the case of simulation rM12, this result is consistent with the fact that retrograde orbits are less destructive than prograde orbits.

The middle right panels of Figs. 6–9 show the velocity dispersion versus formation epoch, with the dash vertical lines indicating the starburst. In 5 of the 8 simulations, the velocity dispersion is larger for stars formed prior to the collision, and smaller for stars born after the collision. This is consistent with the statement that old stars have a smaller rotational support than young stars. The exceptions are the simulations with high mass ratios, M13 and M110, for which σ_V peaks during the starburst, and M12z, for which σ_V peaks after the starburst (Fig. 7).

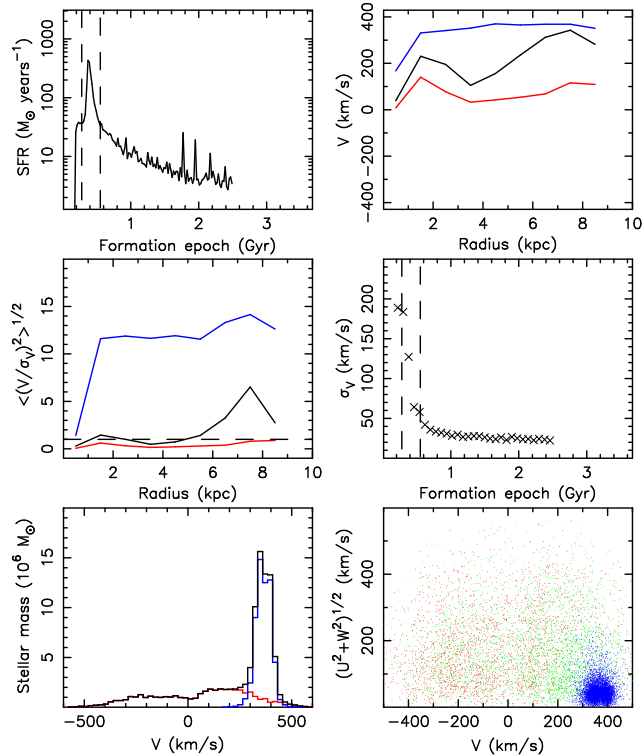


Figure 6. Star formation rate and kinematics for simulation M12. On each panel, the red curves represent old stars, the blue curves and dots represent young stars, and the black curves and dots represent all stars. The vertical dashed lines indicate the beginning and the end of the merger. Top left: star formation rate vs. formation epoch. $t = 0$ corresponds to the beginning of the simulation. Top right: rotation velocity vs. radius for stars located near the plane of the disc ($|Z| \leq 1$ kpc). Middle left: Rotational support versus radius. The dashed line separates rotationally-supported stars (above) from stars supported by velocity dispersion (below). Middle right: velocity dispersion vs. formation epoch. Bottom left: histogram of stellar mass vs. rotation velocity, with negative values indicating counter-rotating stars. Bottom right: Toomre diagram. The black, green, and blue dots indicate stars formed before, during, and after the merger.

The bottom left panels of Figs. 6–9 show histograms of the stellar mass versus rotation velocity. For simulations M12, M12orb, M1290, rM12, and M13, the young population is concentrated in a narrow region of the histogram, while the old population is spread in velocity, from the positive to the negative side (though it is concentrated mostly on the positive side for rM12). The young component is counter-rotating for simulation M11. For simulations M12z, parts of the young component are counter-rotating, and the total distribution is centered near zero. Simulation M110 (the minor merger) differs from all others in that the old population is concentrated at positive velocities. Notice that this is the only case for which the old population is rotationally supported.

One way to discriminate between kinematically different star populations is the use of the Toomre Diagram (Sandage & Fouts 1987). By comparing V (circular velocity) with $U+W$ (radial and perpendicular velocity respectively), we can have a clearer picture of the kinematic distribution

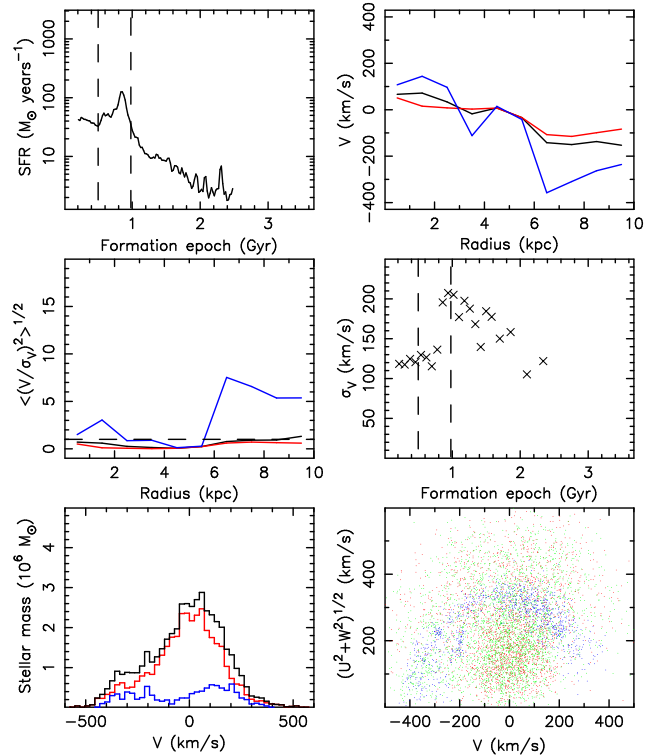


Figure 7. Same as Fig. 6, for simulation M12z.

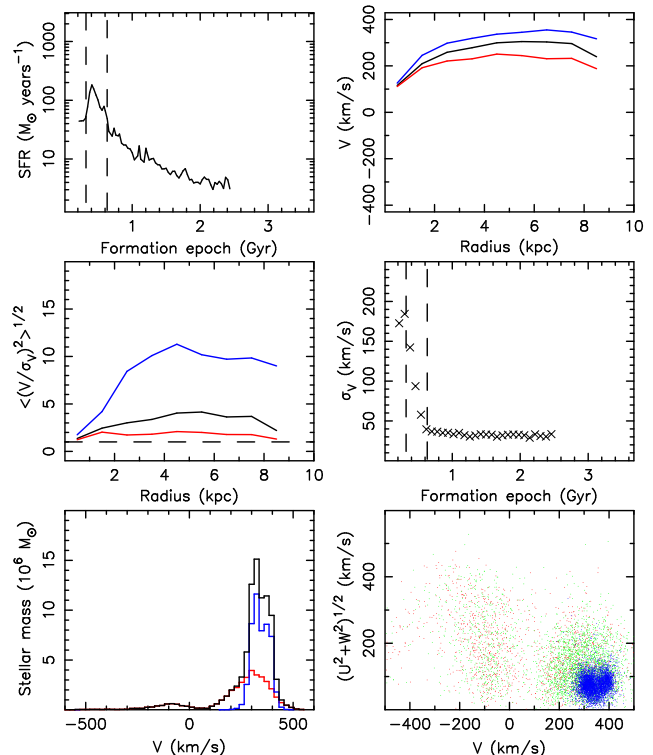


Figure 8. Same as Fig. 6–7, for simulation rM12.

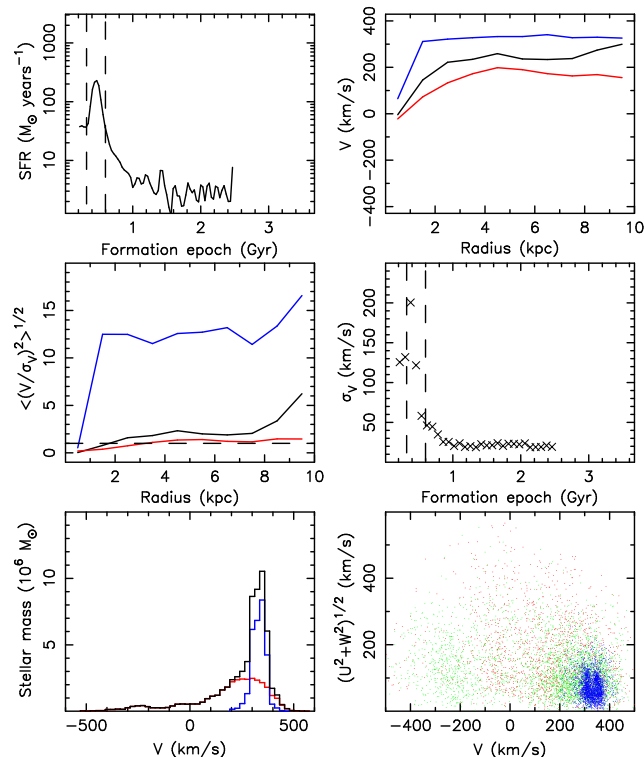


Figure 9. Same as Fig. 6–8, for simulation M13.

of the young and old population. A thin disc will be mostly formed by stars with low $U + W$ and a large V component since all stars will be in nearly coplanar orbits. The bottom right panels of Figs. 6–9 show the Toomre diagram for each simulation. For M12, the young stars are concentrated in a small region of the diagram, centered around $V = 400 \text{ km s}^{-1}$ and $(U^2 + W^2)^{1/2} = 0 \text{ km s}^{-1}$, which is characteristic of a thin disc since these stars are mainly on fast rotating planar orbits. The old stars are distributed throughout the diagram, indicating that these stars follow orbits with significant radial and orthogonal velocities, characteristic of systems supported by velocity dispersion. These stars are located mostly in the thick disc and halo.

The Toomre diagrams for the other simulations show similarities, and also interesting differences, with the diagram for simulation M12. Some simulations present a discontinuity between the positive and negative region of the diagram. For example, simulation rM12 produces two different population of old stars, one forming a thick disc and another one forming a counter-rotating thick disc/halo. Simulation M12z and M11 have a different Toomre diagram than the other simulations. For M12z (Fig. 7), there is no clear disc formed in the remnant, and the young stars are dispersed throughout the diagram. As we saw in the previous section, young stars in this simulation are mostly located in a massive ring around the galaxy. For simulation M11, the young stars in the outer ring are counter-rotating while all stars in the inner disc are co-rotating. For simulation M110, the young population has a significant $(U^2 + W^2)^{1/2}$ component ($\sim 150 \text{ km s}^{-1}$), almost as large as the V component.

We have also performed an analysis of the circularity of the stellar orbits, where $e_j = j_z/j_{\text{circ}}$, and j_z is the z -

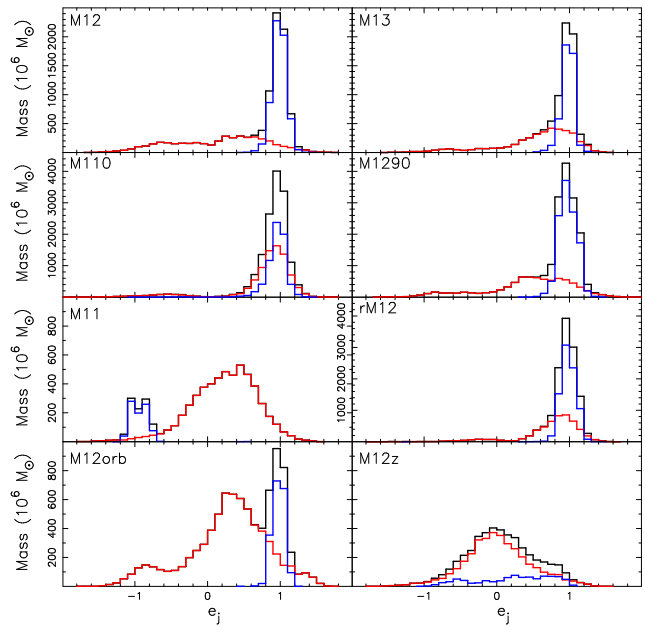


Figure 10. Circularity of the orbits for all simulations. e_j represent the angular momentum of a star particle normalized to a particle in a circular orbit of the same radius. On each panel, the red curves represent old stars, the blue curves represent young stars, and the black curves represent all stars.

component of the specific angular momentum of each star, and j_{circ} is the angular momentum expected for a circular orbit, following the method of Sánchez-Blázquez et al. (2009), which is an approximation of a method used by Abadi et al. (2003). These results are shown in Fig. 10. Simulations M12, M13, M110, M1290, rM12, and M12orb all present a young star population with circular orbits ($e_j \sim 1.0$) and an old population with a high dispersion of circularity. One exception is M110, which presents near circular orbits for both the young and old population, which is expected in a minor merger. Simulations M11 and M12z show non-circular orbits, in good agreement with the other kinematical results. The small thin disc of M11 is also well represented at $e_j \sim -1.0$.

The main conclusion we can draw from the analysis and comparison of the kinematical properties of the remnants is that these kinematical properties, as the structural ones, are strongly dependent of the initial conditions, and support previous results by Robertson et al. (2006).

3.3 Chemical Abundances

As mentioned in the Section I, one of the most important results not yet achieved concerning gas-rich major mergers is their chemical signature. Here we present some of our first results. The chemical properties of all remnants are presented in Figs. 11–18. The top panels show the radial profiles of the α -element abundances $[\alpha/\text{Fe}]$ (calculated by averaging the abundances of O, Mg, and Si) and metallicity $[\text{Fe}/\text{H}]$, calculated by averaging over radial bins. The old population has a higher $[\alpha/\text{Fe}]$ ratio and lower metallicity $[\text{Fe}/\text{H}]$ than the young population, at all radii.

The gradients of $[\alpha/\text{Fe}]$ in the old population are all very

flat. The distributions of $[\alpha/\text{Fe}]$ in the young population are much more complex. In particular, simulations M12, M12z, M1290, and M13 show several local minima and maxima at various radii, with variations as large as 0.5 dex. The gradients of $[\text{Fe}/\text{H}]$ are much smoother. In all simulations except M11, we find a gradient in $[\text{Fe}/\text{H}]$, ranging from -0.01 to -0.1 dex per kpc.

The third rows of panels in Figs. 11–18, show the $[\alpha/\text{Fe}]$ and $[\text{Fe}/\text{H}]$ ratio versus formation epoch. The $[\alpha/\text{Fe}]$ ratio remains fairly constant over time during the merger, and starts decreasing after the merger. The $[\text{Fe}/\text{H}]$ ratio shows a completely opposite behavior: it increases strongly before and during the merger, and keeps increasing, but more slowly, after the merger. This would suggest that the galaxy grows outside-in, with the older, metal-poor stars being located at the outer regions of the disc. To investigate this question, we plot in Fig. 19 the formation epoch of old and young stars versus their final location in the disc, for all simulations. The dashed lines indicate the beginning and the end of the merger. For old stars, the formation epoch either decreases with increasing radius (as in M12) or remains constant (as in M1290). For instance, in the case of M12, stars that formed before the merger are dominant at radius $R > 3$ kpc, while stars that formed during the merger and the associated starburst are more centrally concentrated. The young stars show the opposite trend: the formation epoch increases with radius up to $R = 7.5$ kpc in most simulations. Star-formation after the merger therefore proceeded inside-out. It is the efficiency of chemical enrichment, and not the epoch of star formation, that explains the gradient in $[\text{Fe}/\text{H}]$. Chemical enrichment is more efficient in the center of the remnant, where the stellar density is higher.

The second row of panels in Figs. 11–18 show $[\alpha/\text{Fe}]$ and $[\text{Fe}/\text{H}]$ versus height above the plane. The different extents of the two curves on each panel reflects the different thicknesses of the two discs. Notice that the thin disc is *very thin* in simulation M11, less than 800 pc. There is essentially no vertical gradient in $[\alpha/\text{Fe}]$ for the old population. For the young population, we find a gradient in $[\alpha/\text{Fe}]$ for M12 (0.1 dex per kpc), and possibly another one for M12orb, while there are no evidence for gradients in the other cases. The $[\text{Fe}/\text{H}]$ ratios are either constant, as in simulations M12z and M110, or drops by a factor of order 2 or 3, as in simulations M12 and M1290, for both the old and the young populations. Since the stellar density, and the resulting chemical enrichment, is a much stronger function of radius than height, we naturally expect the vertical gradient of the metallicity to be much weaker than the radial one (Brook et al. 2005).

The most important plots on Figs. 11–18 are the $[\alpha/\text{Fe}]$ versus $[\text{Fe}/\text{H}]$ plots (bottom-left panels). Old stars have larger α -element abundance than young stars, up to a relatively high metallicity ($[\text{Fe}/\text{H}] \simeq -0.5$). We can explain this result by considering the relations between $[\alpha/\text{Fe}]$, $[\text{Fe}/\text{H}]$, and the formation epoch of stars (third-row panels in Fig. 11–18). The metallicity $[\text{Fe}/\text{H}]$ increases with time during the starburst, and levels-off after the starburst is completed. The ratio $[\alpha/\text{Fe}]$ then decreases with time as the metallicity increases, until it reaches the values found in the thin disc. This decrease of $[\alpha/\text{Fe}]$ is slowed near the beginning of the collision, as the starburst leads to a large number of Type II SNe, that enrich the gas in α -elements. After the starburst, Type Ia SNe become effective, and enrich the gas

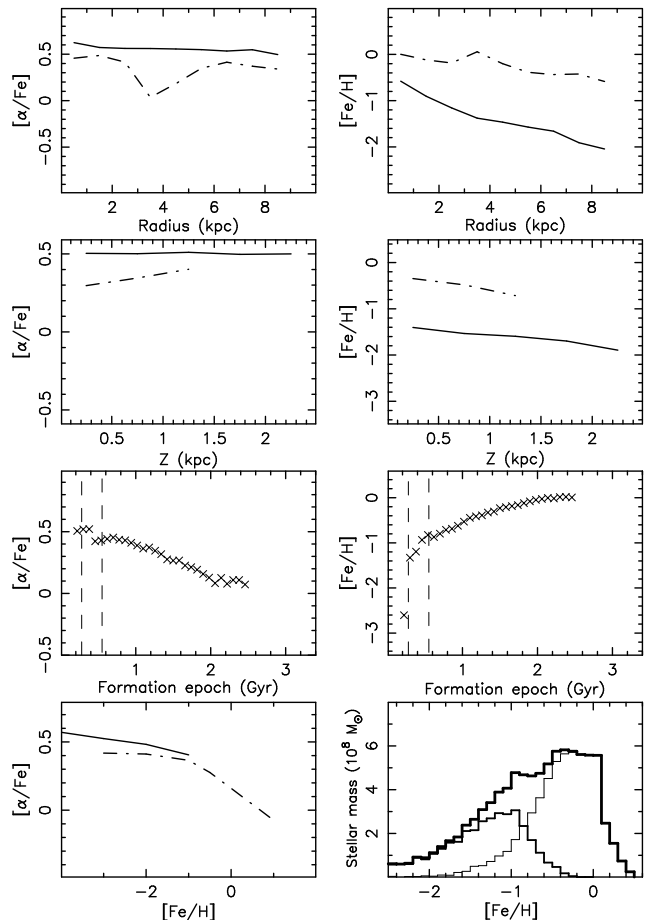


Figure 11. Chemical abundances for simulation M12. On the top four panels and bottom left panel, solid curves represent old stars, and dot-dashed curves represent young stars. The first three rows show the α -elements abundance (left) and metallicity (right) versus radius (first row), height (second row), and formation epoch (third row). Bottom left panel: α -element abundance versus metallicity. Bottom right panel: Stellar mass versus metallicity, for stars born before or after the merger (medium line), after the merger (thin line), and for all stars (thick line).

in iron. This explains why the ratio $[\alpha/\text{Fe}]$ gradually decreases after the collision.

We complete this study by calculating the stellar mass in metallicity bins, for both populations. The results are shown in the bottom right panels of Figs. 11–18. Old and young stars have different metallicity distributions. The old population peaks in the range $[\text{Fe}/\text{H}] = [-1.0, -0.6]$, while the young population peaks in the range $[\text{Fe}/\text{H}] = [-0.4, 0.4]$. This implies that old stars are formed, on average, by gas that has not yet been enriched by a large number of nearby Type Ia SNe. We can gain more insight into this process by plotting Toomre diagrams for different metallicity bins. The results for simulation M12 are shown in Fig. 20. We recall that the concentration of stars in the region $V \simeq 400$ km/s, $(U^2 + W^2)^{1/2} \simeq 0$ km/s represents the thin disc, and the remainder of the diagram represents the thick disc and the halo. Low-metallicity stars ($[\text{Fe}/\text{H}] < -3$) are located in the halo, high-metallicity stars ($[\text{Fe}/\text{H}] > 0$)

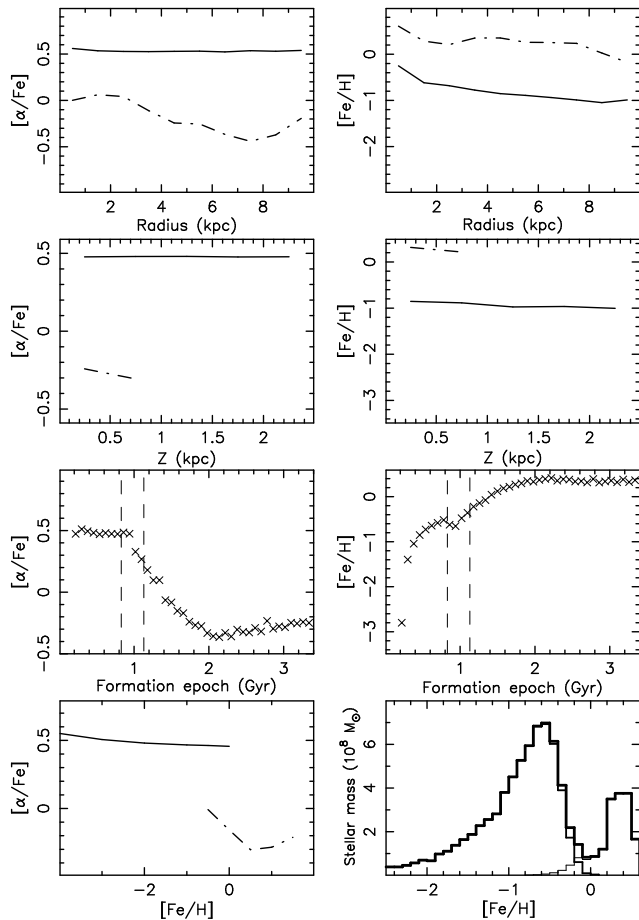


Figure 12. Same as Fig. 11, for simulation M12orb

are located in the thin disc, and intermediate-metallicity stars are found in both locations.

The main result we draw from this analysis of the chemical abundance is that the merger leaves a clear signature: the old stars, located in the thick disc and the halo, have a ratio $[\alpha/\text{Fe}]$ that remains constant with increasing $[\text{Fe}/\text{H}]$ up to high metallicities ($[\text{Fe}/\text{H}] = -0.5$), while the young stars, located in the thin disc, have a lower ratio $[\alpha/\text{Fe}]$ which decreases with increasing metallicities. This result is very robust: we found it in each of the 8 simulations included in our study, including the minor merger (simulation M110).

Early gas-rich mergers in our simulations occur, by construction, prior to the timescale for significant Type Ia SNe pollution. Ultimately, this is responsible for the robustness of our results.

4 DISCUSSION

The results presented in this paper support the gas-rich merger scenario as a way to explain the formation of large disc galaxies in the Universe. Our results agree very well with the kinematical results of Robertson et al. (2006). That said, the gas-rich process may be necessary to form a disc, but it is not a sufficient condition. We can see this in our two simulations which formed bulge-dominated galaxies, namely M11 and M12z. Explaining this difference is not simple be-

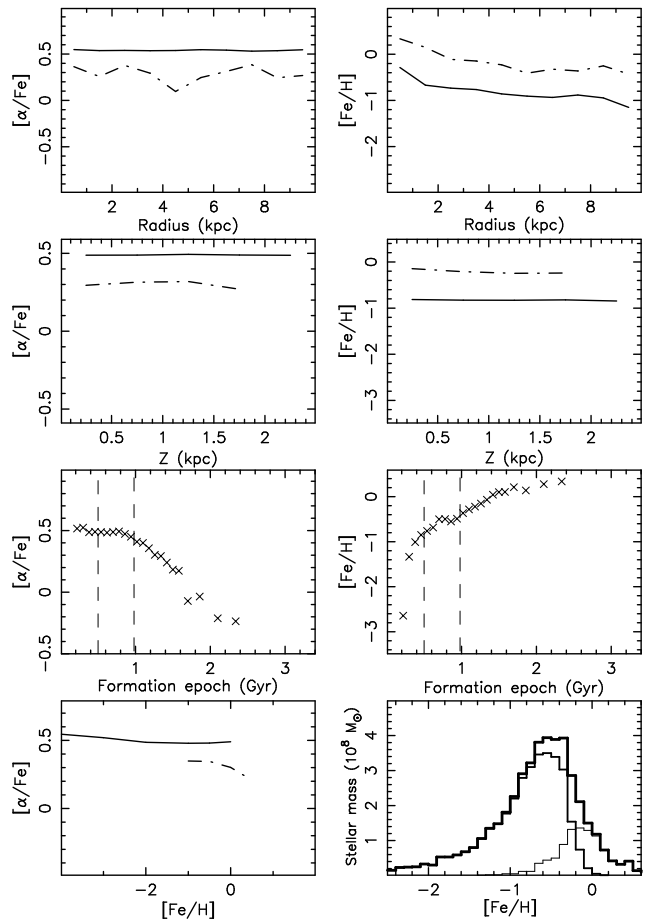


Figure 13. Same as Fig. 11–12, for simulation M12z

cause of the chaotic nature of the merger process. There is likely a complex relationship between the initial conditions and the behavior of the gas during the merger. The duration of the merger and the violence of the collision seems to favor a higher dynamical warming, and this favors the formation of a small rotationally supported disc, embedded within a large spheroidal component. In the case of simulation M11, the two progenitors have a lower mass than in the others simulations, but the starburst has the same intensity. As a result, there is not enough gas left after the merger to form a substantial thin disc. This agrees with the results of Robertson et al. (2006) who found that low-mass progenitors are more likely to form an important spheroidal component than high-mass ones.

When a disc-like remnant is formed, it invariably consists of two disc components: a thick disc made of stars formed before or during the merger, and a thin disc made of stars born after the merger. The thick disc has a lower rotation velocity than the thin disc, in agreement with the findings of Yoachim & Dalcanton (2006). The scale-length ratio between the two components is also in agreement with this work, which suggests that gas-rich disc mergers may be a common way to form disc galaxies. However, we have to be careful since subsequent gas infall from satellites or the intergalactic medium is not included in our simulations. Such gas infall could increase the scale-length of the thin disc and affect our results (see, e.g., Brooks et al. 2009). Stars belong-

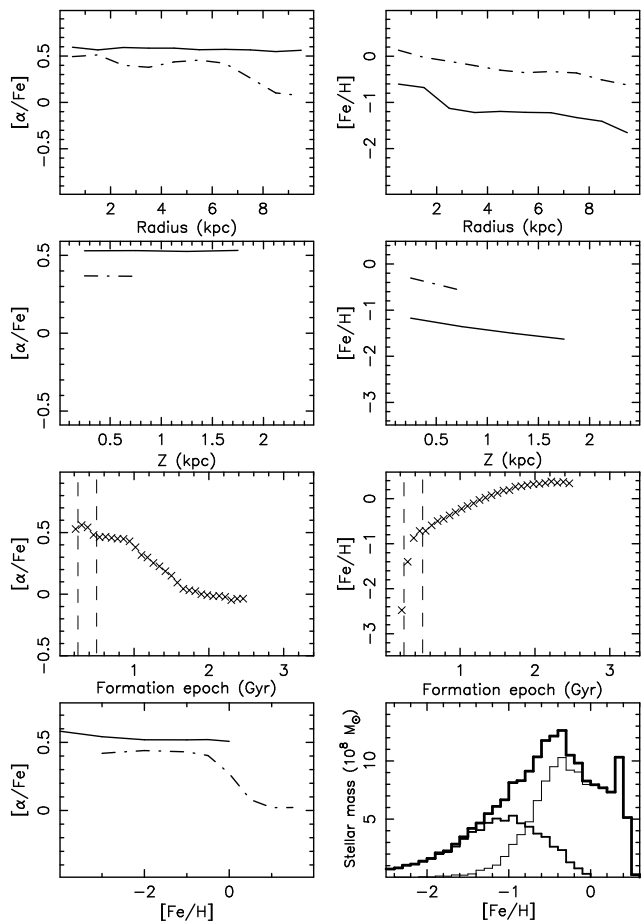


Figure 14. Same as Fig. 11–13, for simulation M1290.

ing to the thick and thin discs differ by their abundances in various metals. Old stars have an excess in α -elements relative to young stars at metallicities $[\text{Fe}/\text{H}]$ below -0.5 . This result is in good agreement with observational studies on the chemical abundances of the two disc components of the Milky Way, if the old and young stars in our simulations are analogous to the thick- and thin-disc stars, respectively. Reddy, Lambert, & Allende Prieto (2006) published a spectroscopic survey of 176 stars with high probability to be part of the galactic thick disc, selected with the *Hipparcos* catalog. These authors analyze the relationship between the abundances of 22 chemical elements and the $[\text{Fe}/\text{H}]$ ratio. It is clear from their Fig. 12 that the $[\alpha/\text{Fe}]$ ratio is higher for the thick disc than the thin disc by almost 0.15 until the metallicity reaches $[\text{Fe}/\text{H}] = -0.3$. At larger metallicities, the $[\alpha/\text{Fe}]$ ratios of the two discs becomes similar. The authors explain this fact by invoking an extended period of enrichment in iron by Type Ia SNe, an explanation that is supported by our work. Fig. 16 in the same article shows that chemical elements other than the α -elements do not follow the same pattern, which is further evidence of the important role of Type II SNe in the formation of the Milky Way, and support the scenario that a major collision took place in the history of the Milky Way.

Another similar study was done by Bensby et al. (2005). That study presents abundances for 102 dwarf F and G stars, and uses their kinematics to determine if they belong

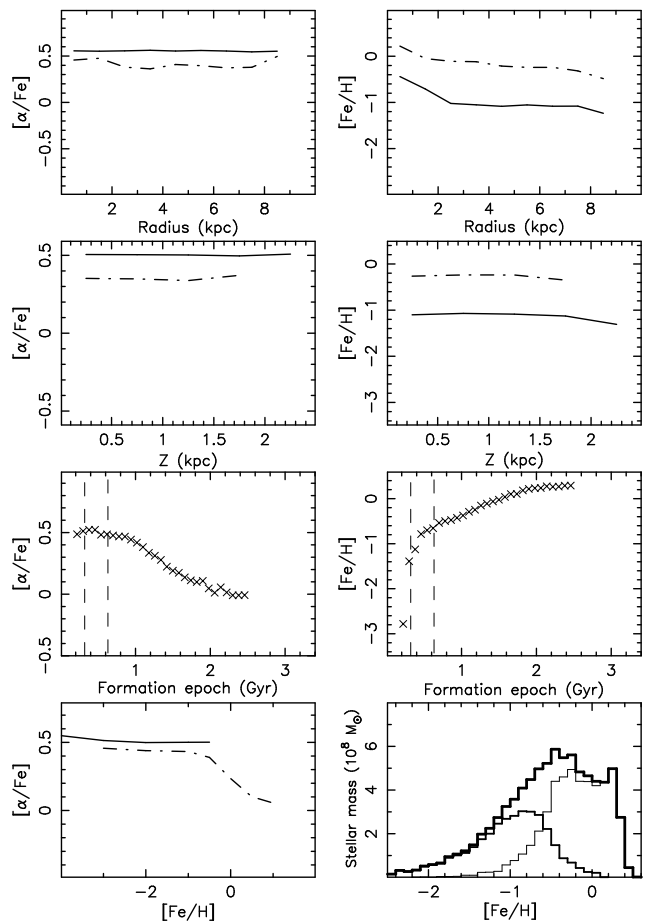


Figure 15. Same as Fig. 11–14, for simulation rM12.

to the thin or thick disc. Their Fig. 8 shows the abundances of oxygen, magnesium, and silicon as functions of metallicity, which indicates that stars in the thick and thin disc have different abundances for a metallicity $[\text{Fe}/\text{H}] < -0.5$. Their Fig. 10 is particularly interesting and shows that the abundance of oxygen decreases with increasing metallicity in the interval $-1.0 < [\text{Fe}/\text{H}] < 0.0$. This is all in agreement with the results presented here. These authors suggest the existence of several observational constraints related to the formation and chemical evolution of the thick disc:

- Thick-disc stars and thin-disc stars have different chemical abundances.
- For a $[\text{Fe}/\text{H}]$ smaller than a certain value, thick disc stars have a larger abundance of α -elements than thin-disc stars.
- The ratio $[\alpha/\text{Fe}]$ decreases with increasing $[\text{Fe}/\text{H}]$, which shows the important contribution of Type Ia SNe.
- Stars in the thick disc are on average older than stars in the thin disc.

Our results mostly agree with these constraints, which supports the gas-rich, major-collision scenario for the formation of the thick disc of the Milky Way, a scenario in which a collision leads to an intense starburst accompanied by a very large number of Type II SNe. These SNe enrich the gas supply in α -elements, allowing the formation of stars with a high $[\alpha/\text{Fe}]$ ratio. The starburst also leads to a progressive

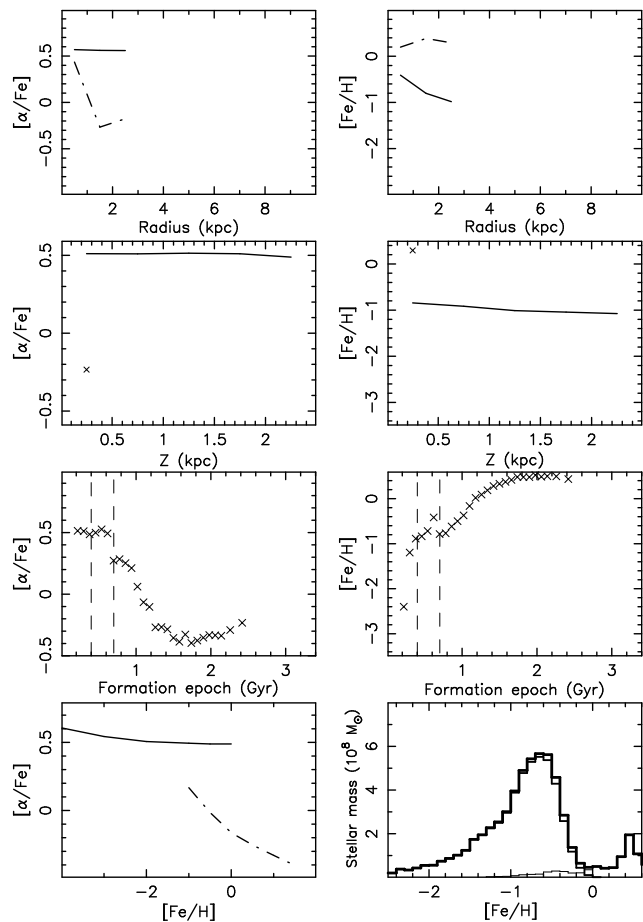


Figure 16. Same as Fig. 11–15, for simulation M11. We could not calculate vertical profiles for the young stars, because the thin disc is too thin. Instead we indicate the mean values of $[\alpha/\text{Fe}]$ and $[\text{Fe}/\text{H}]$ with a single symbol (\times) in the second-row panels.

enrichment in iron caused by Type Ia SNe. Stars formed after the collision will therefore have a smaller $[\alpha/\text{Fe}]$ for the same metallicity. These stars will form a thin disc with a smaller velocity dispersion than the stars formed during the merger. Another interesting result is the drop in $[\text{Fe}/\text{H}]$ with increasing radius.

Finally, we must point out that the initial conditions used in our study are greatly simplified. First, the initial conditions do not include a spheroidal component made of stars. We assume that the merger progenitors are pure disc for simplicity. We might expect that these stars, if included, would end up in the halo of the final galaxy, which might explain that most simulations produced a low-mass halo. We can argue that our results are valid in the limit where the initial spheroidal components are too small to affect the dynamics of the collision. We have not included a bulge component as well. Although morphologies of high redshift galaxies are unknown, this assumption may be too simplistic and our results may be biased by this assumption. However, a recent work showed the presence of a bulge can produce a disc remnant with a gas ratio as low as 12% (Barnes 2002). These facts are an evidence that a merger between bulgeless disc-disc galaxies is not a sufficient condition to form a dick remnant. In fact, bulgeless mergers

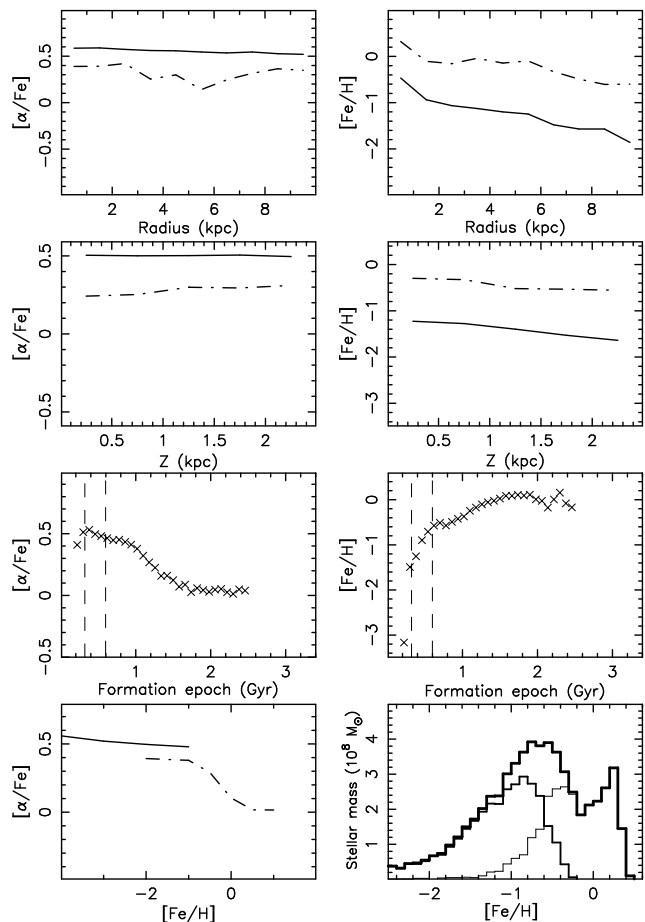


Figure 17. Same as Fig. 11–16, for simulation M13

generally produce elliptical remnants in dissipationless simulations (González-García & Balcells 2005). So, the presence of a massive gaseous component is probably the major condition to reform a disc after a major merger. We also have to add that the softening length used in this study is slightly higher than what are used in the recent state-of-the-art simulations. However, the morphological aspects of our study show good agreement with previous such higher spatial resolution simulations, showing that the resolution is sufficient for the analysis presented in this paper.

The hierarchical model of structure formation normally includes a significant amount of collision and accretion of low-mass galaxies. It is presumptuous to assume that the formation of the thick disc can be explained entirely by one single collision. It is possible that several of these collisions take place in the initial phases of the formation of spiral galaxies (Brook et al. 2005; Conselice 2006). Nevertheless, our study can explain several observations with the important starburst that takes place during a major, gas-rich collision.

5 SUMMARY AND CONCLUSION

Using GCD+, we have performed 8 simulations of major mergers between gas-rich spiral galaxies. We have analyzed the kinematic, structural, and chemical properties of stars

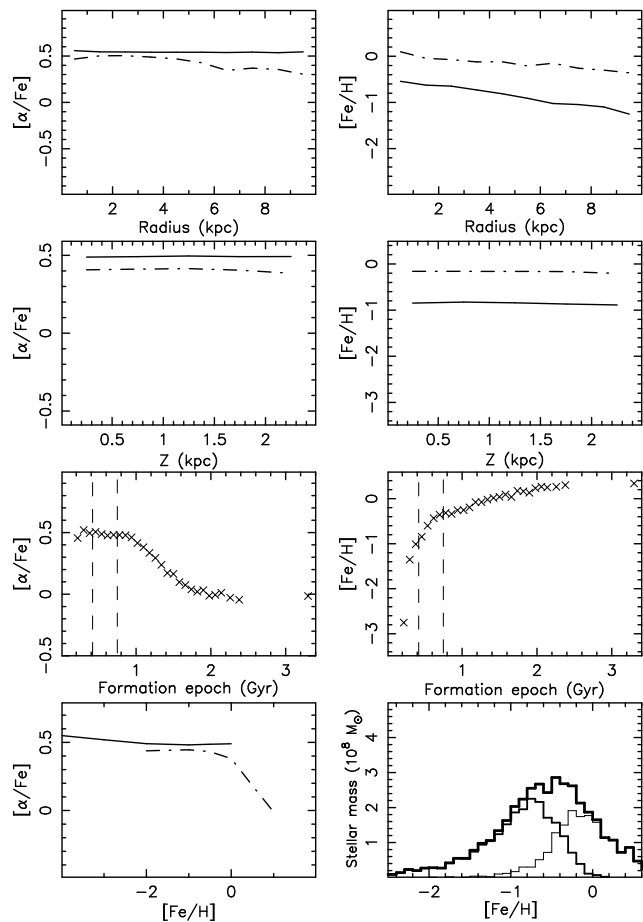


Figure 18. Same as Fig. 11–17, for simulation M110

formed before and during the collision (the old population) and stars formed after the collision (the young population). We used the star formation rate to define these two populations. A fraction of the old stars end up in the halo of the merger remnant, while the remaining stars form a thick disc which is partly supported by velocity dispersion, partly supported by rotation, and sometimes includes a significant counter-rotating component. The young stars form a thin disc that is supported by rotation, and, in many cases, a ring that might or might not be coplanar with the thin disc. The discs themselves tend to be coplanar, the angle between them being $\sim 6^\circ$ or less. With rare exceptions, both discs are well-fitted by an exponential profile, and the scale-length of the thick disc exceeds the one of the thin disc a few percents up to a factor of 1.60.

The starburst occurring during the collision rapidly enriches the gas in various metals. Explosions of Type II SNe follow rapidly the start of the collision, owing to the short lifetime of their progenitors, and enrich the intergalactic medium in α -elements. Enrichment by Type Ia SNe is spread over a large period of time, enabling the enrichment in iron of both stellar populations, which results in an old population having a $[\alpha/\text{Fe}]$ ratio higher than the young population, even at relatively large metallicities ($[\text{Fe}/\text{H}] = -0.5$). This could explain the high $[\alpha/\text{Fe}]$ ratio observed in stars in the thick disc and the halo of the Milky Way. This result do

not depend strongly upon the initial conditions, since it was found in all simulations.

Our main conclusion is that the morphological, kinematical and chemical properties of the thick and thin disc can be reproduced in a scenario where thick disc formed in a gas rich merger between two disc galaxies. Furthermore, while the structural and kinematical properties of the merger remnants are strongly dependent on the initial conditions – features such as the ratio of the disc scale-lengths, the extent of the discs, the presence of rings or of a counter-rotating component, vary from simulation to simulation – the chemical abundances show a remarkable consistency among the various simulations. The key result of this study is that the ratio $[\alpha/\text{Fe}]$ remains constant with increasing $[\text{Fe}/\text{H}]$ for old stars, up to $[\text{Fe}/\text{H}] = -0.5$ while it decreases with increasing metallicity for young stars. This is true in each of the 8 simulations we considered. The observed chemical signatures in our merger remnants require that mergers happen before the onset of the majority of Type Ia SNe, regardless of the orbits or mass ratios of the progenitors. Furthermore, the mergers need to be gas rich to lead to a remnant with a rotationally supported disc. These characteristics are consistent with the mergers we expect to find at high redshift and, therefore, our results support this scenario for the formation of the different disc components in the Milky Way.

ACKNOWLEDGMENTS

The simulations were performed at the Laboratoire d’Astrophysique Numérique, Université Laval, the University of Central Lancashire’s High Performance Computing Facility, and at the Center for Computational Astrophysics of the National Astronomical Observatory of Japan. The code used for generating the entries displayed in Table 4 was written by Keven Roy. SR, & HM acknowledge the support of the Canada Research Chair program and NSERC. PSB acknowledges the support of a Marie Curie Intra-European Fellowship within the 6th European Community Framework Programme. BKG and CBB acknowledge the support of the UK’s Science & Technology Facilities Council (ST/F002432/1) and the Commonwealth Cosmology Initiative.

REFERENCES

- Abadi, M. G., Navarro, J. F., Steinmetz, M., & Eke, V. R. 2003, *ApJ*, 591, 499
- Barnes, J. E. 2002, *MNRAS*, 333, 481
- Barnes, J. E. , & Hernquist, L. 1992, *ARA&A*, 30, 705
- Barnes, J. E. , & Hernquist, L. 1996, *ApJ*, 471, 115
- Bekki, K. 1998, *ApJ*, 502, L133
- Bekki, K., & Shioya, Y. 1998, *ApJ*, 497, 108
- Bekki, K., & Shioya, Y. 1999, *ApJ*, 513, 108
- Bensby, T., Feltzing, S., Lundström, I., & Ilyin, I. 2005, *A&A*, 433, 185
- Blumenthal, G. R., Faber, S. M., Primack, J. R., & Rees, M. J. 1984, *Nature*, 311, 517
- Brook, C. B., Kawata, D., Gibson, B. K., & Flynn, C. 2004a, *MNRAS*, 349, 52

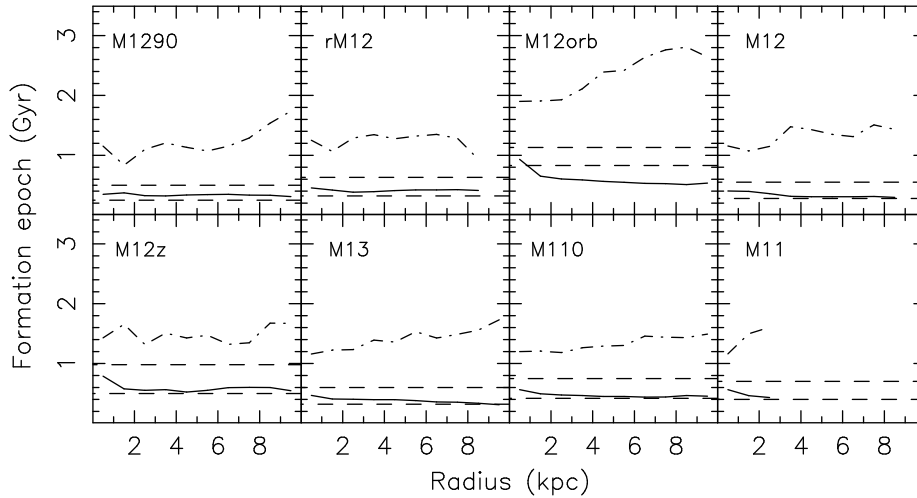


Figure 19. Star formation epoch versus final radius for old stars (solid line) and young stars (dot-dashed line), for the 8 simulations. The horizontal dashed lines indicate the beginning and the end of the starburst.

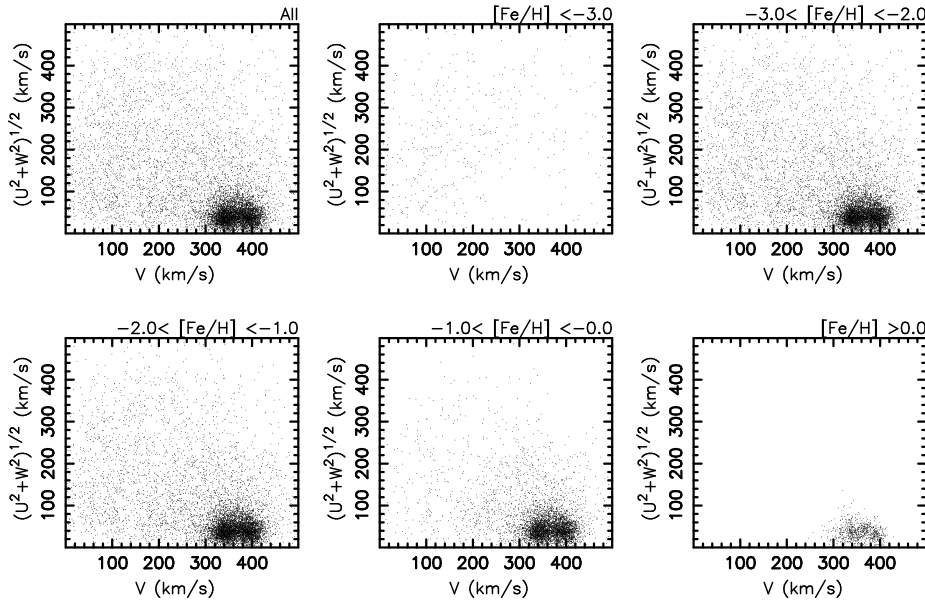


Figure 20. Toomre diagram for stars located near the disc plane ($Z < 1$ kpc), for simulation M12, divided according to metallicity. The metallicity range is indicated on top of each panel.

Brook, C. B., Kawata, D., Gibson, B. K., & Freeman, K. C. 2004, *ApJ*, 612, 894
 Brook, C. B., Gibson, B. K., Martel, H., & Kawata, D. 2005, *ApJ*, 630, 298
 Brook, C. B., D. Kawata, Martel, H., Gibson, B. K., & Bailin, J. 2006, *ApJ*, 639, 126
 Brook, C., Richard, S., Kawata, D., Martel, H., & Gibson, B. K. 2007, *ApJ*, 658, 60 (B07)
 Brooks, A. M., Governato, F., Quinn, T., Brook, C. B., & Wadsley, J. 2009, *ApJ*, 694, 396
 Chiba, M., & Beers, T. C. 2000, *AJ*, 119, 2843
 Conselice, C. J. 2006, *ApJ*, 638, 686
 Cox, T. J., Jonsson, P., Primack J. R., Somerville R. S. 2006, *MNRAS*, 373, 1013
 Cox, T. J., Jonsson, P., Somerville R. S., Primack J. R.,

Dekel, A. 2008, *MNRAS*, 384, 386
 Dalcanton, J. J., & Bernstein, R. A. 2002, *AJ*, 124, 1328
 Delhaye, J. 1965, in *Galactic Structure*, eds. A. Blaauw & M. Schmidt (Chicago: University of Chicago Press), p. 61
 Elmegreen, B. G., & Elmegreen, D. M. 2006, *ApJ*, 650, 644
 Erb, D. K., Steidel, C. C., Shapley, A. E.; Pettini, M., Reddy, N. A., & Adelberger, K. L. 2006, *ApJ*, 647, 128
 Evans, N. W., 1993, *MNRAS*, 260, 191
 Fall, S. M., & Efstathiou, G. 1980, *MNRAS*, 193, 189
 González-García, A. C., & Balcells, M. 2005, *MNRAS*, 357, 753
 Ghigna, S., Moore, B., Governato, F., Lake, G., Quinn, T., & Stadel, J. 2000, *ApJ*, 544, 616
 Gilmore, G., Wyse, R. F. G., & Jones, J. B., 1995, *AJ*, 109, 1095

- Gilmore, G., Wyse, R. F. G., & Kuijken, K., 1989, *ARA&A*, 27, 555
- Governato, F., Brook, C. B., Brooks, A. M., Mayer, L., Willman, B., Jonsson, P., Stilp, A. M., Pope, L., Christensen, C., Wadsley, J., & Quinn, T. 2008, arXiv:0812.0379
- Hernquist, L. 1992, *ApJ*, 400, 460
- Hernquist, L. 1993, *ApJ*, 409, 548
- Hernquist, L., Weil, M. L. 1993, *MNRAS*, 261, 804
- Hernquist, L., & Mihos, J. C. 1995, *ApJ*, 448, 41
- Hopkins, P. F., Cox, T. J., Younger, J. D., & Hernquist, L. 2008, arXiv:0806.1739
- Iwamoto, K., Brachwitz, F., Nomoto, K., Kishimoto, N., Umeda, H., Hix, W. R., & Thielemann, F.-K. 1999, *ApJS*, 125, 439
- Jing, Y. P., & Suto, Y. 2000, *ApJ*, 529, L69
- Johansson, P. H., Naab, T., Burkert, A. 2009, *ApJ*, 690, 802
- Jurić, M., et al. 2008, *ApJ*, 673, 864
- Kawata, D., & Gibson, B. K. 2003a, *MNRAS*, 340, 908
- Kawata, D., & Gibson, B. K. 2003b, *MNRAS*, 346, 135
- Kazantzidis, S., Bullock, J. S., Zentner, A. R., Kravtsov, A. V., & Moustakas, L. A. 2008, *ApJ*, 688, 254
- Kazantzidis, S., Zentner, A. R., & Bullock, J. S. 2008, in *The Galaxy Disk in Cosmological Context* (IAU Symposium No. 254), eds. J. Andersen, J. Bland-Hawthorn, & B. Nordstrom (Cambridge University Press), arXiv:0807.2863
- Klypin, A., Kravtsov, A. V., Bullock, J. S., & Primack, J. R. 2001, *ApJ*, 554, 903
- Kobayashi, C., Tsujimoto, T., & Nomoto, K. 2000, *ApJ*, 539, 26
- Kodama, T., & Arimoto, N. 1997, *A&A*, 320, 41
- Komatsu, E., et al. 2009, *ApJS*, 180, 330
- Kuijken, K., & Dubinski, J. 1995, *MNRAS*, 277, 1341
- Kroupa, P. 2002, *MNRAS*, 330, 707
- López-Sanjuan, C., Balcells, M., Pérez-González, P.G., Barro, G., García-Dabó, C.E., Gallego, J., & Zamorano, J. 2009, arXiv:0905.2765
- Mapelli, M., Moore, B., Giordano, L., Mayer, L., Colpi, M., Ripamonti, E., Callegari, S. 2008, *MNRAS*, 383, 230
- McGaugh, C. C. 2005, *ApJ*, 632, 859
- Mihos, J. C., & Hernquist, L. 1996, *ApJ*, 464, 641
- Moore, B., Quinn, T., Governato, F., Stadel, J., & Lake, G. 1999, *MNRAS*, 310, 1147
- Naab, T., Burkert, A., & Hernquist, L. 1999, *ApJ*, 523, L133
- Naab, T., & Burkert, A. 2003, *ApJ*, 597, 893
- Naab, T., Jesseit, R., & Burkert, A. 2006, *MNRAS*, 372, 839
- Navarro, J. F., Frenk, C. S., & White, S. D. M. 1996, *ApJ*, 462, 563
- Navarro, J. F., Frenk, C. S., & White, S. D. M. 1997, *ApJ*, 490, 493
- Okamoto, T., Eke, V. R., Frenk, C. S., Jenkins, A., 2005, *MNRAS*, 363, 1299
- Quinn, P. J., Hernquist, L., & Fullagar, D. P. 1993, *ApJ*, 403, 74
- Reddy, B. E., Lambert, D. L., & Allende Prieto, C. 2006, *MNRAS*, 367, 1329
- Robertson, B., Bullock, J. S., Cox, T. J., Di Matteo, T., Hernquist, L., Springel, V., & Yoshida, N. 2006, *ApJ*, 645, 986
- Robertson, B. E., & Bullock, J. S. 2008, *ApJL*, 685, L27
- Sánchez-Blázquez, P. et al. 2009, *A&A*, 499, 47
- Sandage, A., & Fouts, G. 1987, *AJ*, 93, 74
- Spergel, D. N. et al., 2007, *ApJS*, 170, 377
- Springel, V. 2000, *MNRAS*, 312, 859
- Springel, V., & Hernquist, L. 2005, *ApJ*, 622, L9
- Springel, V., Di Matteo, T., Hernquist, L., 2005, *MNRAS*, 361, 776
- Stewart, K. R., Bullock, J. S., Wechsler, R. H., Maller, A. H., & Zentner, A. R. 2008, *ApJ*, 683, 597
- Stewart, K.R., Bullock, J. S., Wechsler, R. H., Maller, A. H. 2009, arXiv:0901.4336
- Thacker, R. J., & Couchman, H. M. P. 2000, *ApJ*, 545, 728
- Toomre, A., 1977, in *Evolution of Galaxies and Stellar Populations*, eds. B. M. Tinsley & R. B. Larson, (New Haven: Yale University Observatory), p. 401
- Toomre, A., & Toomre, J. 1972, *ApJ*, 178, 623
- van den Hoek, L. B., & Groenewegen, M. A. T. 1997, *A&AS*, 123, 305
- White, S. D. M., & Rees, M. J. 1978, *MNRAS*, 183, 341
- Woosley, S. E., & Weaver, T. A. 1995, *ApJS*, 101, 181
- Yoachim, P., & Dalcanton, J. J. 2006, *AJ*, 131, 226

This paper has been typeset from a \TeX / \LaTeX file prepared by the author.